GNSS-Based Passive Radar Sensing Using Hybrid-Aperture System

Randy Silver, Yan (Rockee) Zhang, Hernan Suarez, Yu Pan and Yih-Ru Huang

Intelligent Aerospace Radar Team (IART)
University of Oklahoma,
Norman, OK 73072
http://uas.ou.edu

ABSTRACT

A hybrid-aperture radar system is being developed for passive, GNSS-based sensing and imaging missions. Different from previous work, the real aperture (RA) array has excellent cross-range resolution and electronic scanning capability, and synthetic aperture processing is applied for the dimension along the UAV/aircraft flight path. The hybrid aperture thus provides real-time, combined sensing capability and multiple functions. Multi-level signal synchronization and tracking is used to ensure the signal phase coherency and integrity. The advantages of covert radar sensing and reduced onboard computing complexity of this sensor are being demonstrated through experiments.

KEYWORDS: GNSS, Radar, Software Defined Radio /Radar (SDR)

1. INTRODUCTION

The concepts and initial development of a *passive radar* operating at RF frequencies with the capabilities to receive aviation and GNSS band *signals of opportunity*, from the non-cooperative transmitters and is able to adaptively select sources from multiple propagation paths, is presented. The sensor is designed to intelligently "harvest" useful information about hazards/threats on the ground, or even generate radar images of them. Since the transmitters are located elsewhere, the passive radar can actually achieve the cost and power requirements for small, tactical Unmanned Aerial Vehicle (UAV) deployment.

For the safety and survivability of ISR platforms, stealth or covert surveillance is critical to reduce the EM signatures. (1) Optical sensors would lose feasibility during non-ideal weather conditions, so passive surveillance at RF is going to be important to future operations. (2) Passive radar is a key solution to spectrum sharing and management challenges. (3) C-SWaP consideration: The passive radar does not need high-power transmitters so the cost, size, weight and power are reduced. The smallest active UAS radar transceiver system on the market today has the size of about 7 inches by 7 inches, and consumes about 15 watt power. For Tier I and II UAVs, however, this is still big and heavy and thus limits the usage of radar in UAS. (4) Application of software-defined radar and radio (SDRR) combination. Passive radar requires the receivers be much more agile, intelligent and function-diversified (combination of navigation, communication and radar signal processing) than existing active radars.

Previous work of space-surface Bi-static SAR (SS-BSAR) in UK [1-3] has demonstrated the feasibility of GNSS-based passive radar sensing and initial imaging results with Galileo. However, these results are not sufficient to convince the community the realistic performance of GNSS (GPS) -based radar image quality, due to the lack of hardware capabilities. There are also many difficulties have not been fully addressed in this technology. First, extremely low SNR of GNSS signal reflection from ground targets (less than -140 dBm/Hz) requires good antenna gain and directivity. The multi-path reflection from different sources can also be interferences, if focused images are needed. Second, commercial GPS receivers do not contain radar signal detection capability, and third, maintaining phase coherence through multiple GPS receive channels for high-quality imaging is difficult in general.

The above challenges motive us to investigate a hybrid aperture solution with software-defined (SD) GPS radar receivers. The following sections discuss the detailed system concept, engineering design, antenna system design and receivers. Initial measurement data with target signature extractions is also presented.

Radar Sensor Technology XVII, edited by Kenneth I. Ranney, Armin Doerry, Proc. of SPIE Vol. 8714, 871409

2. SYSTEM CONCEPT AND DESIGN

2.1 Hybrid Sensing and Imaging Geometry

A simple downward imaging geometry can be explained here as an example. More complicated imaging geometries can be discussed as next steps. In Figure 1, the UAV is flying along Y-direction, and the physical array is installed along the wing direction. The GPS C/A code can be wiped out by correlation and demodulation. The navigation message can also be removed by synchronizing with a direct GPS receiver. Thus the collected signal within the synthetic aperture time turns to be coherent single tone signal that can be converted down to base band for further processing. Half wavelength spaced L band antenna elements are distributed along the wing facing down to the ground. This nadir view gives the best range resolution at a fixed altitude. The UAV flies at relatively low altitude constrained by the GPS signal power budget. A normal GPS receiver will be onboard for reference. The antenna array will be facing zenith and it needs to have very low back lobes to avoid multi-path interference. The stop-and-go mode is assumed. At least one complete period of C/A code needs to be collected for correlation. This means several milliseconds are needed when the receiver "stops" to collect data. The Doppler shift caused by the high-speed orbiting satellite can be estimated by the reference GPS receiver, and compensated in collected data. The GPS satellite has antenna featuring wide beam width, thus the imaging area can be assumed to be constantly and uniformly illuminated when the aperture is being synthesized.

For the coordinates and parameters shown in Figure 2.1.1, the reflected signal from the ground can be written as

$$s(u,v) = \sum_n s_n(u,v) = \sum_n \sigma_n \, e^{-jk\sqrt{h^2+(x_n-u)^2+(y_n-v)^2}}, \quad (1)$$

where *n* is number of scatterers on the ground, and only the baseband portion is shown.

The signal is essentially a *two dimensional array* signal. The beam steering vector is

$$\hat{e} = \frac{(x,y,0)}{\sqrt{x^2+y^2}} \quad (2)$$

The propagation path difference at each array element is

$$d(u,v) = \hat{e} \cdot (u,v,h) = \frac{xu+yv}{\sqrt{x^2+y^2}} \quad (3)$$

The beam will be steered to a particular point in the cross-range if the path differences are all compensated to the same value so that the returned signal can be summed constructively, giving the reconstructed image as

$$S_b(x,y) = \sum_{u,v} s(u,v) e^{-jkd(u,v)} \quad (4)$$

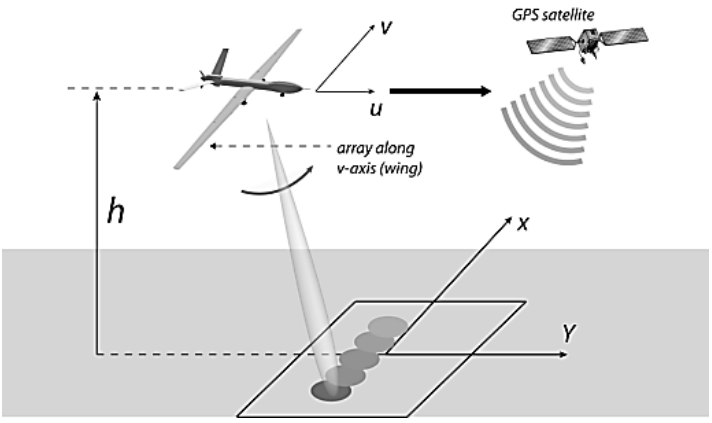

Figure 1: Downward-Looking imaging geometry from an UAV platform.

The image above can be formed equivalently by either performing actual array beamsteering or 2D matched filtering in digital domain. By applying advanced beamforming processing and using controlled flight path, it is also possible to achieve GNSS-based passive Synthetic Aperture Radar (SAR) and GMTI capability. Figure 2 shows some initial simulation results of GPS-based passive imaging. It was assumed that one complete cycle of C/A codes at L1 (1.575 GHz) frequency is collected (several milliseconds in length). The Doppler shift caused by the high-speed orbiting satellite can be estimated by the direct GPS receiver, and compensated in collected data.

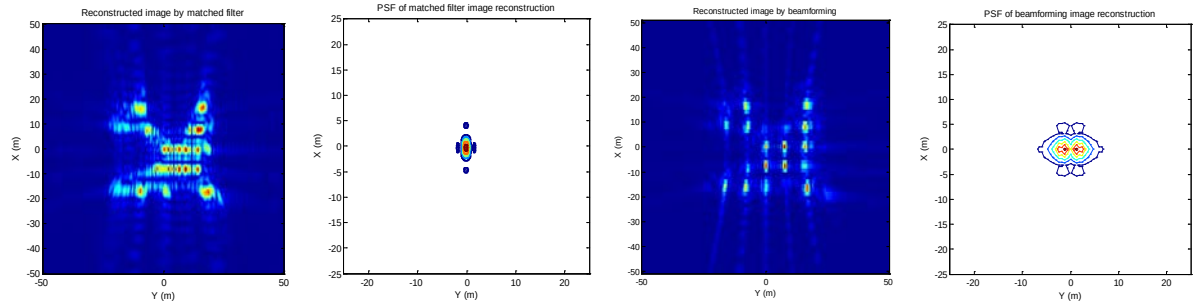

(a) **(b)** **(c)** **(d)**

Figure 2: Simulated images of an aircraft parking on the ground, *reflected GPS L1 signal is used as bi-static radar waveform*. UAV has wingspan of 2 m and flight height of 50 m. Targets are distributed symmetrically in 100m ×100m area. Linear physical array has 1.9m aperture and synthetic array has 9.5 m aperture length. (a) Result image using frequency-domain 2D matched filter, (b) The Point-Spread-Function (PSF) of point target with matched filtering, (c) Result image using the antenna array beamforming technique, (d) PSF with array beamforming. The achieved ground resolution is about 5m × 5m in average.

2.2 Link Budget and System Design Consideration

A rough link budget developed in[5] and based upon the signal received by a linearly polarized antenna, with 3-dB gain, is shown in Table 1.

Table 1: L1-Band C/A Code Link Budget for a Linearly Polarized Antenna with 3-dB Gain.

User minimum received power	-158.5 dBW (-128.5 dBm)
User linear antenna gain	3.0 dB
Free space propagation loss (FSPL)[1]	184.4 dB
Total atmospheric loss	0.5 dB
Polarization mismatch loss	3.4 dB
Required satellite EIRP[2]	26.8 dBW (56.8 dBm)
Satellite antenna gain at 14.3^{O}, worst-case BLK II off-axis angle (dB)	13.4 dB
Required minimum satellite antenna input power	13.4 dBW (43.4 dBm or 21.9 W)

The proposed system differs from the link budget developed in Table 1 in that the GNSS-based passive radar receives reflected GPS signals. These signals scatter from the ground, buildings, cars, etc. Thus, the user minimum received power is lower than stated in Table 1. It can be demonstrated that the reflected power normalized to the direct power can be calculated as,

[1] FSPL is calculated as $L_{fs} = 10log_{10}[\frac{4\pi r^2}{\lambda^2}]$, found in *Radar Handbook,3rd edition* by Merrill I. Skolnik

[2] Effective Isolated Radiated Power; defined (in dB) as EIRP = Power Transmitted + Gain of the Transmitter, see *Antenna Theory and Design, 2nd edition* by Warren L. Stultzman and Gary A. Thiele

$$P_{R,refl} = \frac{\sigma A G_{R,refl}}{4\pi R^2 G_{R,dir}}, \qquad (5)$$

where $P_{R,refl}$ is the normalized power received that is reflected to the received direct power, σ is the reflectivity per unit area, A is the area of the reflecting surface (i.e. the resolution of the radar), $G_{R,refl}$ is the gain of the receiving antenna on the reflected channel, $G_{R,dir}$ is the gain of the direct receiving antenna, and R is the distance from the receiving antenna to the reflecting surface. Using the previous formula and assuming σ = 1 and A = 1 m^2, R is 300m above ground level, and the satellite elevation is arbitrarily at an angle of 58^O, Lindgren states that the maximum reflected power is -16 dB down from the direct signal.

The received power will also depend on satellite elevation angle and antenna pattern. The Interface Specification IS-GPS-200 shows that received power will vary by approximately 2 dBW depending on GPS satellite vehicle elevation angle, with a max occurring between 45-60 degrees above the horizon. [4] explains that GPS satellites are designed to have a double-peak beam pattern to cover the surface visible to the respective satellite.

Depending on the reflectivity and area of the reflection source, a good estimate for the losses incurred due to reflection is 20 dB. Accordingly, the antenna system developed is designed to have an antenna gain of approximately 20 dB to offset receiver loss from reflections, shown in Figure 3. The system will also not incur losses from polarization mismatch because the antenna system will be left-hand circularly polarized. Therefore, the antenna system will receive, at a minimum, a signal power of -158.1 dBW (-128.1 dBm).

Per the above equation, the higher the altitude at which the UAV travels, the lower the power received by a 1/R^2, of which we need to take caution during flight tests. On a positive note, however, objects with higher reflectivity will increase the reflected power the antenna system receives. Thus, the potential targets will greatly impact our ability to create any image.

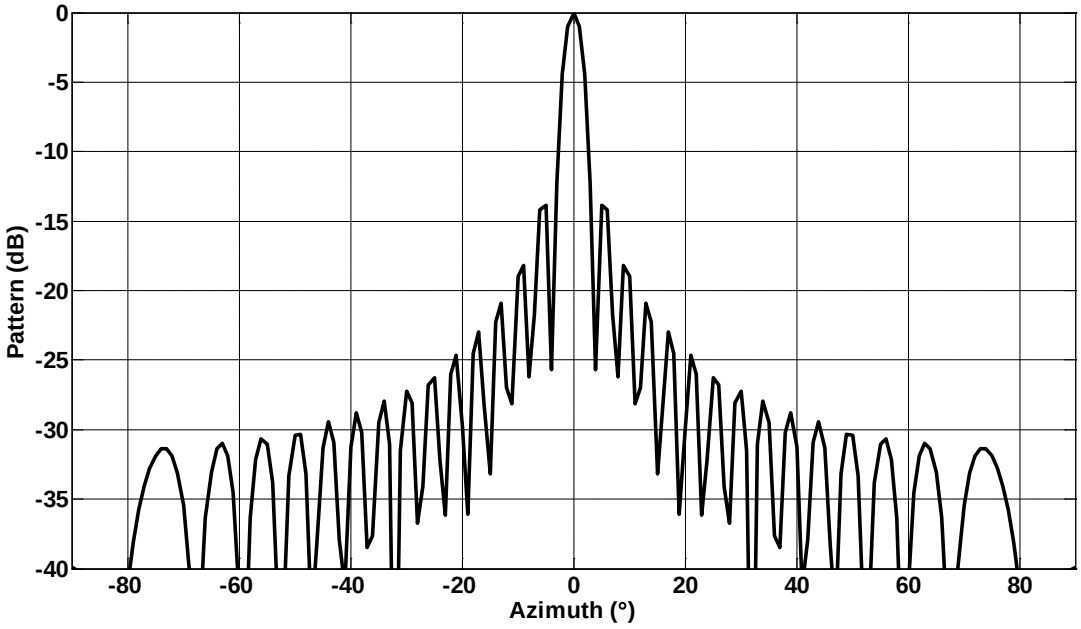

Figure 3: Array Antenna Pattern Simulation: Note the antenna gain of approximately 20 dB and 3-dB Beamwidth of 3.16 degrees.

2.3 System Architecture

The concept of using both synthetic aperture (SA) and real aperture (RA) array in the GNSS-based passive radar observations has been mentioned before but a seamless combination of two apertures in real-time observation has not been demonstrated. A hybrid aperture system consisting of an electronic scanning array at GPS frequency band and synthetic array processing is being developed by the University of Oklahoma. The radar adapts both downward looking and side-looking modes. For downward looking mode, the electronic scanning array antenna scans through the cross-range direction and perform synthetic aperture processing for signal received along flight path at the same time. The key challenge of GNSS-based processing is signal synchronization, which is achieved at both the hardware level (containing two synchronized software receivers and a WAAS receiver providing Time and Space Position Information (TSPI) in real time for the reference) and software level (precise code/phase-tracking, UTC time decoding and local template generation technique). The current real aperture array contains 32 active elements and scans in azimuth direction with about 3 degree beam resolution, and the software-defined GPS receivers are modified to perform radar image formation and target detection. In addition to the covertness of ISR operation and reduced SWaP, the significant advantages of the hybrid aperture system include reduced computational complexity of onboard processor, good phase coherency, integration with GNSS navigation system and potential multiple functionalities.

Figure 4 shows the diagram of the complete passive radar system for ground test, the initial design is completed in late 2012 and currently the hardware system is completed. The software is developed to run on multiple inter-connected PC platforms with both Linux and Windows OS. The GPS signal sampler is a mixed-signal ASIC (SiGe 4120) from SiGe with internal RF receiver chain and ADCs, currently uses GPS-L1 signals. Initial data with this system is being collected and analyzed at the Radar Innovations Lab of OU.

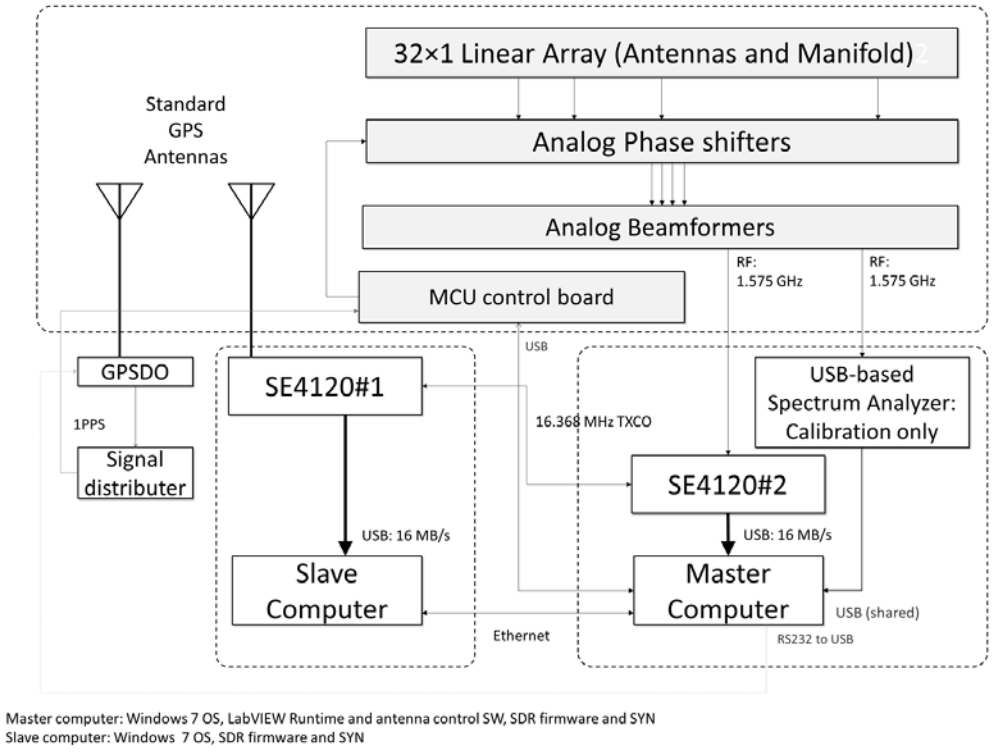

Figure 4: The complete GPS-radar hardware system diagram.

3. ARRAY ANTENNA DESIGN

The configuration of the pin-feed microstrip antenna with a left-hand circular polarization is shown in Figure 5. The antenna consists of a patch, a coaxial probe, a dielectric substrate layer, and a backed ground plane. The optimized parameters of the antenna are shown in Figure 5. Triangles are cut on the two corners of the patch to generate the circular polarization. Rogers TMM10i is used as the substrate, with a dielectric constant $\varepsilon_1 = 9.8$. The antenna is designed to operate at 1.575 GHz, and is simulated with the commercial software CST-Microwave Studio. The fabricated antenna elements are also measured using an Agilent PNA network analyzer, and the measured reflection coefficients are shown in Figure 6. Measurement results indicate that the antennas have a center frequency around 1.575 GHz and usable bandwidth about 15 MHz.

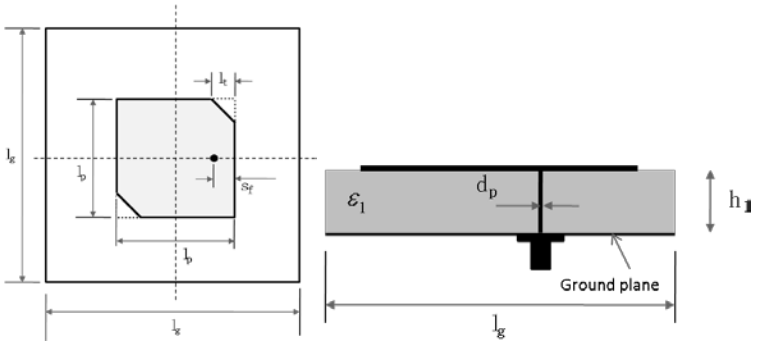

l_p	29.01 mm
l_g	87.029 mm
l_t	2.055 mm
s_f	11.09 mm
d_p	1.27 mm
h_1	3.175 mm
ε_1	9.8

(a) **(b)** **(c)**

Figure 5: Configuration of the antenna element. (a) Top view of the antenna, (b) Side view of the antenna, (c) Parameters and values of the antenna.

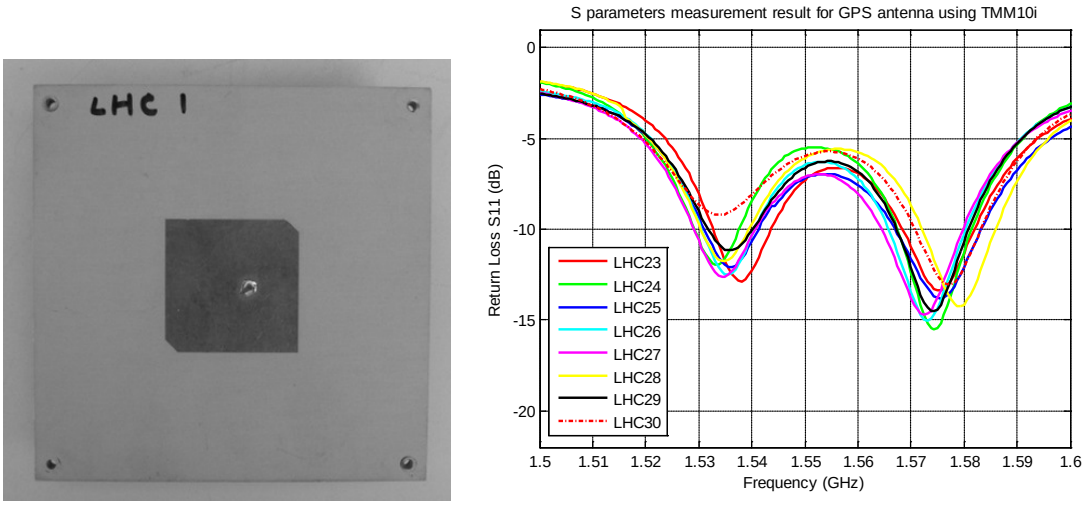

(a) **(b)**

Figure 6: (a) Fabricated antenna element, (b) Measured reflection coefficients of the antennas.

The array system consists of 32 of the aforementioned antenna patches arranged in a linear array, spaced 9 cm (or 0.4726λ) apart. The antenna patches' outputs are fed into our Automatic Beam Former (ABF). The ABF, shown in Figure 7, consists of 32 RF phase-shifters manipulated by an mBed-controlled DAC from Analog Devices, which

provides the necessary voltage levels to the analog phase shifters. The outputs of the ABF are then separated into 4, 8-to-1 power combiners, which are then fed into one 4-to-1 power combiner, where the final output of the array system is given to a software-defined receiver (SDR) for sampling and formatting for a USB connection to pass and to store the data on a PC. The array system, excluding the mBed-controlled DAC/power supply and SDR, is mounted on a 10 feet (3.048 m) aluminum U-channel and weighs approximately 40 pounds (approx. 18 kg). The system was tested for antenna pattern at the Radar Innovations Lab with the testing area shown in Figure 8. The antenna pattern taken from these outdoor tests is shown as Figs 9 and 10 demonstrate the ABF's electronic beamsteering capabilities.

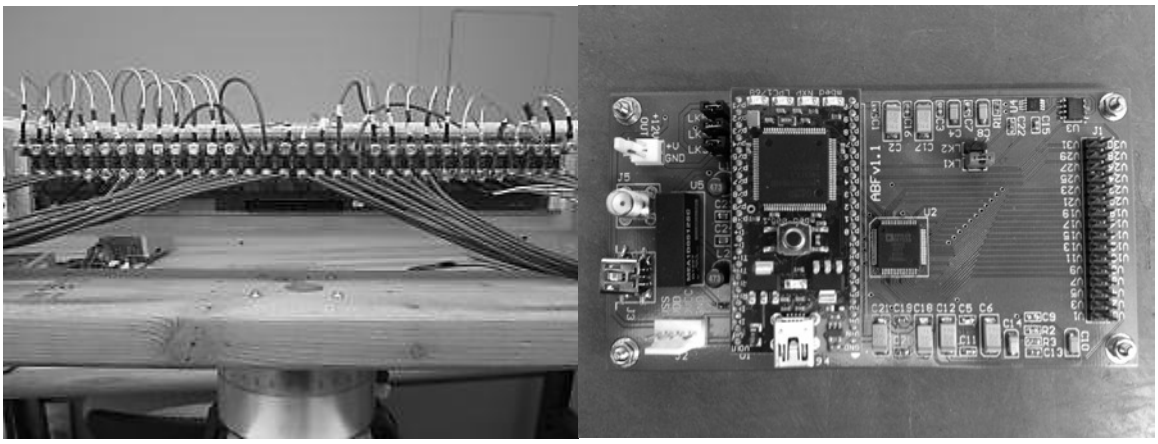

(a) **(b)**

Figure 7: The Automatic Beam Former (ABF) System, (a) Analog phase-shifters shown with antenna system connections, (b) mBed-controlled DAC with power supply. The components shown in (a) and (b) are connected by a ribbon cable, which carries the appropriate voltage levels for the phase-shifters.

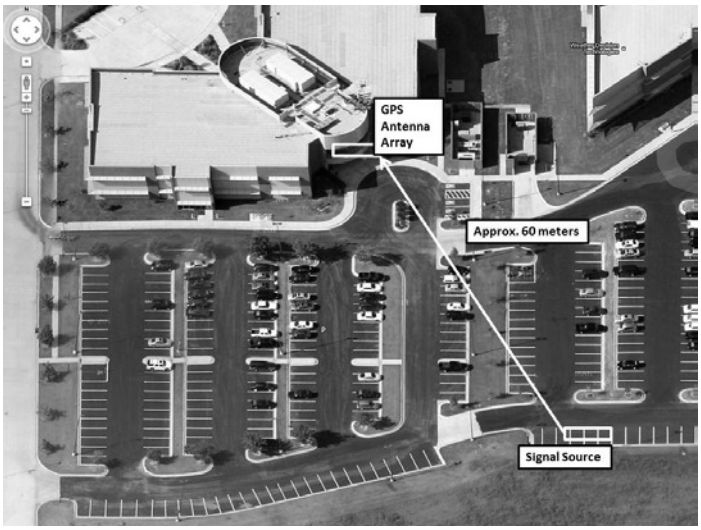

Figure 8: Antenna Pattern and Beam Steering Testing Area at the Radar Innovations Laboratory in Norman, OK.

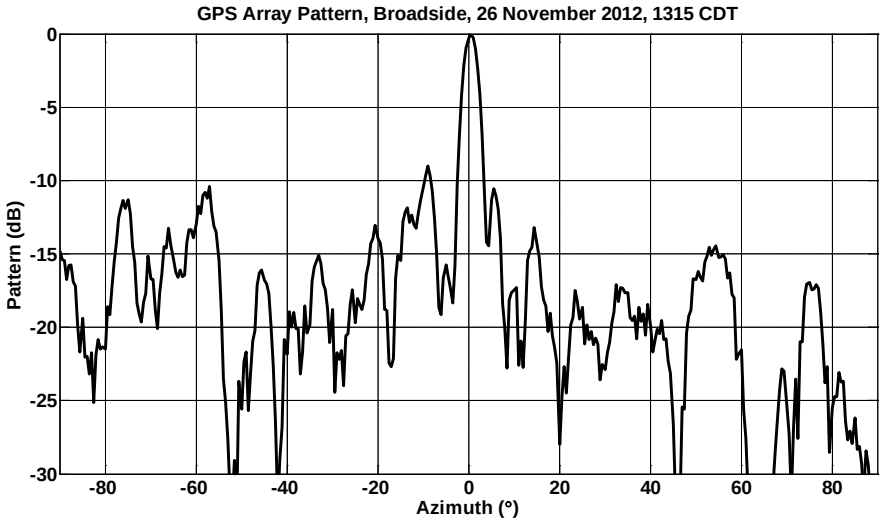

Figure 9: The passive radar electronic scanning antenna, (a) photos in the passive GPS array system being tested on a campus building deck, (b) measured receive array pattern (with a linear-polarized L-1 beacon) at the broadside.

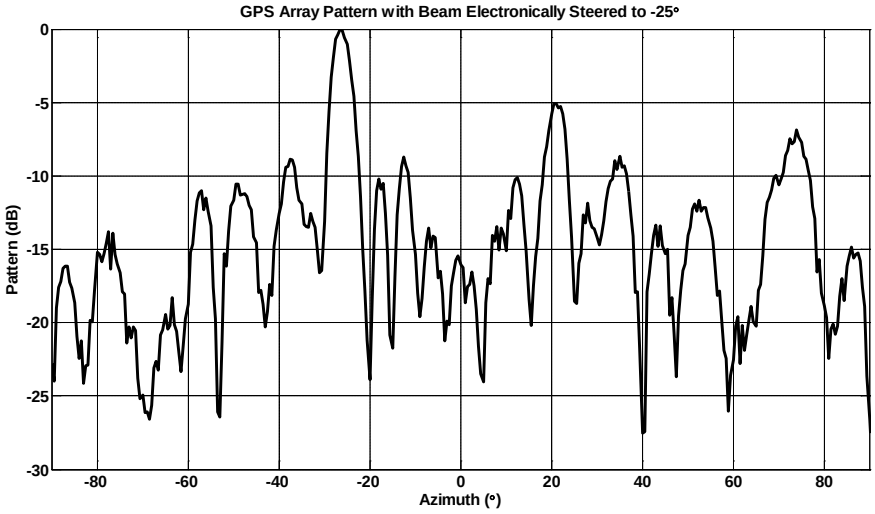

Figure 10: Electronic Beam-Steering demonstration, -25^{o} off broadside.

4. SOFTWARE-DEFINED GPS RADAR RECEIVER

The received GPS signals are sampled and processed for storage using a Software-Defined Receiver (SDR), which is coupled with the remaining components of the GPS Radar Hardware, form the Software-Defined GPS Radar Receiver, shown in Figure 11 with major components labeled. Detailed by Figure 12, the received GPS signals from the GPS Array and Reference channels are sampled and sent to the PCs for storage and further processing. The signed binary data from the Reference channel are subtracted from the GPS Array for noise reduction, and then processed using MATLAB code to acquire and track the signal. The tracking outputs (In-Phase and Quadrature prompt, early, and late code) are used to generate real-aperture images and to determine raw pseudo-ranges. If more than 4 satellites are acquired, further signal processing to decode the navigation data is possible, which generates SV location, receiver location, corrected pseudo-ranges, and time information.

Briefly, the MATLAB code used to process the received GPS signals is detailed in uses the parallel code phase search algorithm to acquire the SVs, which consists of removing the carrier from the I and Q signal, then correlating the I and Q data with a local PRN replica to create a power metric for threshold analysis, after which a second run produces a second maximum for normalization. Finally, to track the acquired SVs, the data is demodulated and mixed to baseband, where the data are sent through a PLL to track the carrier frequency and a DLL to track the code to produce In-Phase and Quadrature early, late, and prompt code for correlation analysis.

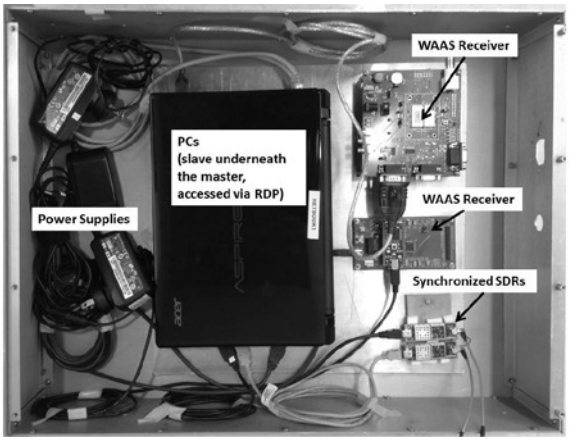

Figure 11: Software-Defined GPS Radar Receiver.

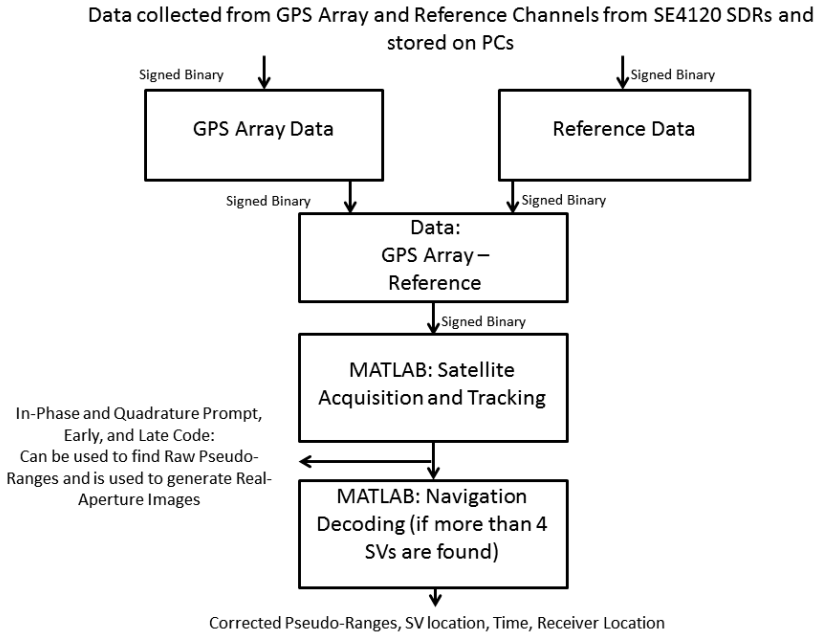

Figure 12: Signal Processing Flow Graph.

5. INITIAL DATA COLLECTION AND ANALYSIS

5.1 GROUND TEST: University of Oklahoma Research Campus

On 22 February 2013, we took our GPS Array Bi-static Radar to the roof of the National Weather Center (NWC) in Norman, OK to collect data for target identification and rudimentary real-aperture imaging. Figure 13 is a sky view of the NWC and some of the targets used for identification and also roughly plots the scanning area of the two data collection tests.

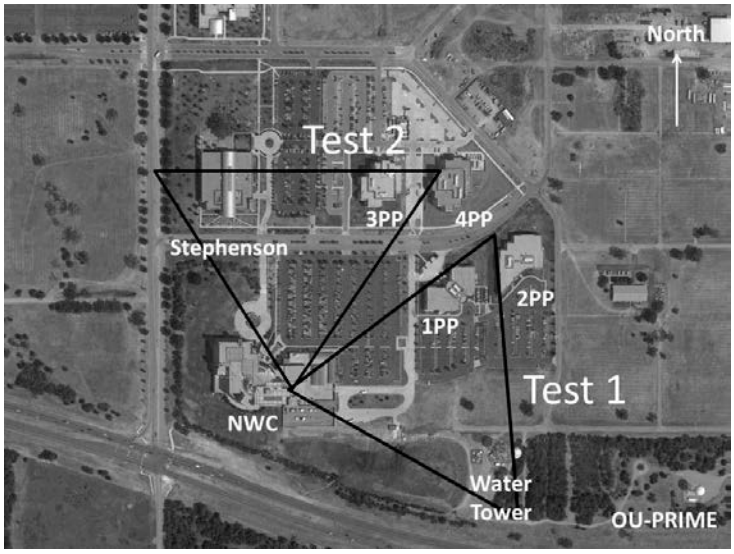

Figure 13: Sky View of the University of Oklahoma Research Campus: Testing took place on the roof of the NWC.

The results from Test 1 and Test 2 are shown as Figure 14 and Figure 15, respectively, along with point-of-view pictures of the respective testing areas and sky charts denoting the SV's locations.

(a)

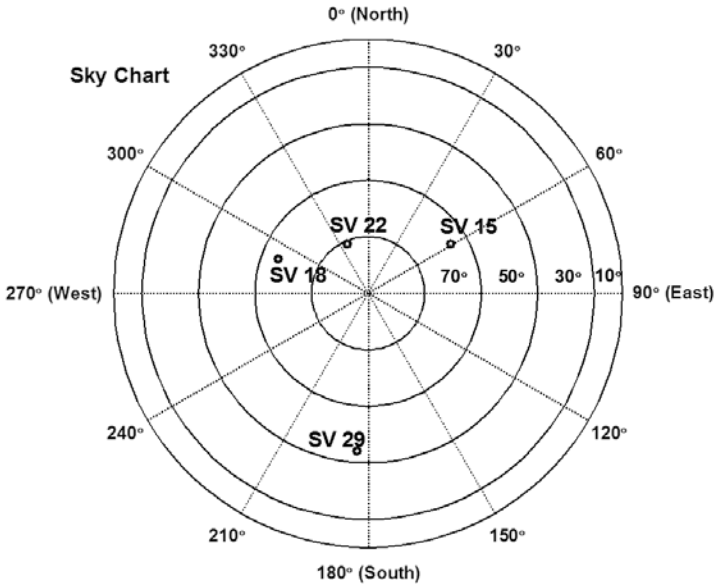

(b)

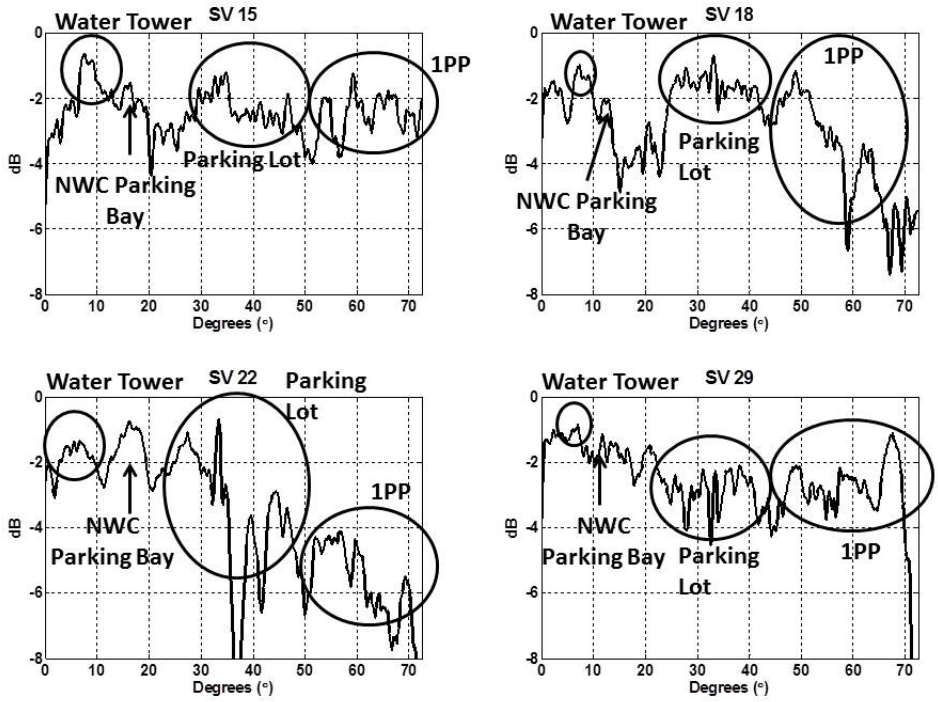

(c)

Figure 14: Test 1 results: (a) Point-of-View of Testing Area, scanned from right to left; (b) SV locations; (c) Relative Powers of specific SVs, normalized in dB.

In Test 1, the major targets are identified in Figure 14(a) (east of the NWC) and the SVs used for data collected are identified in Figure 14(b). Figure 14(c) is a plot of the relative powers normalized in dB, with a scan from right to left of Figure 14(a). Notice that SVs 15, 18, and 22 have a peak in the first 10 seconds of data collection, corresponding to the water tower, with SV 15 showing more distinctly the separation of the water tower and the parking lot. SV 29 has a peak in the last 10 seconds as the satellite was behind the array and reflecting off of 1PP at this point in the data collection. Also note the spread of the peaks from SV 22. SV 22 is almost directly overhead creating many reflections received by the large horizontal beamwidth.

(a)

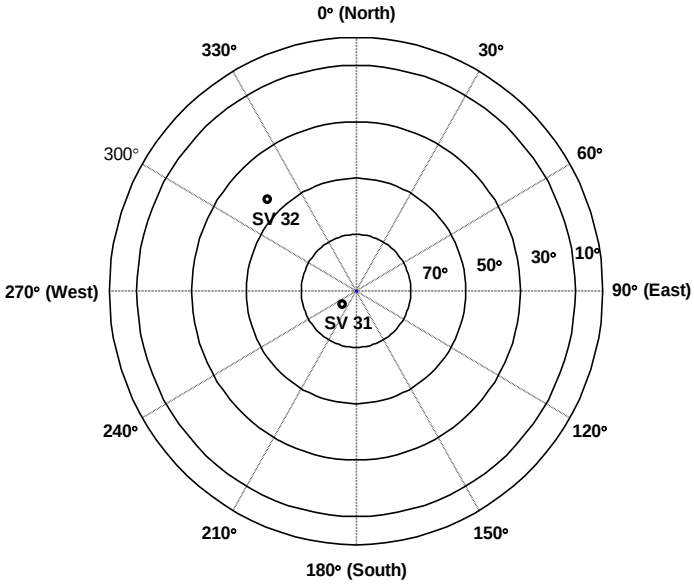

(b)

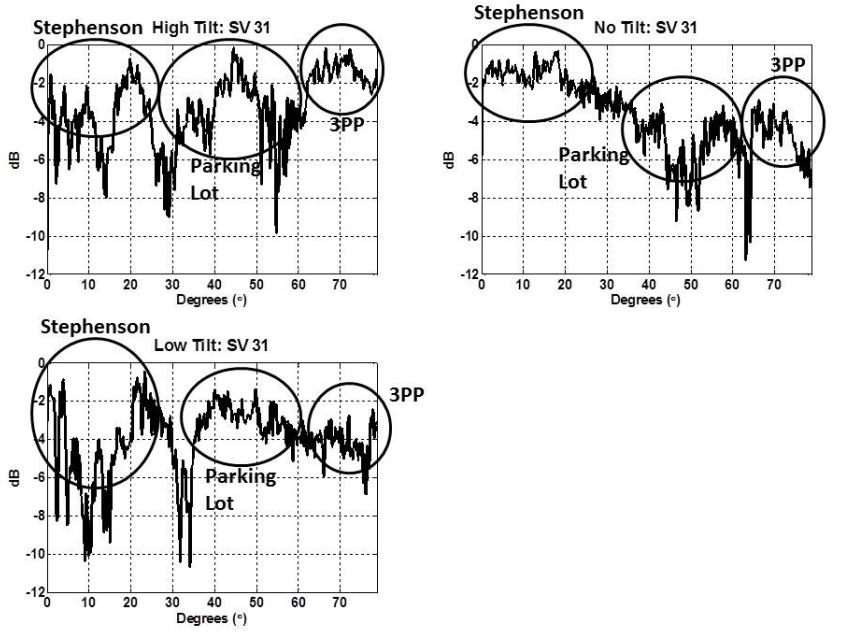

(c)

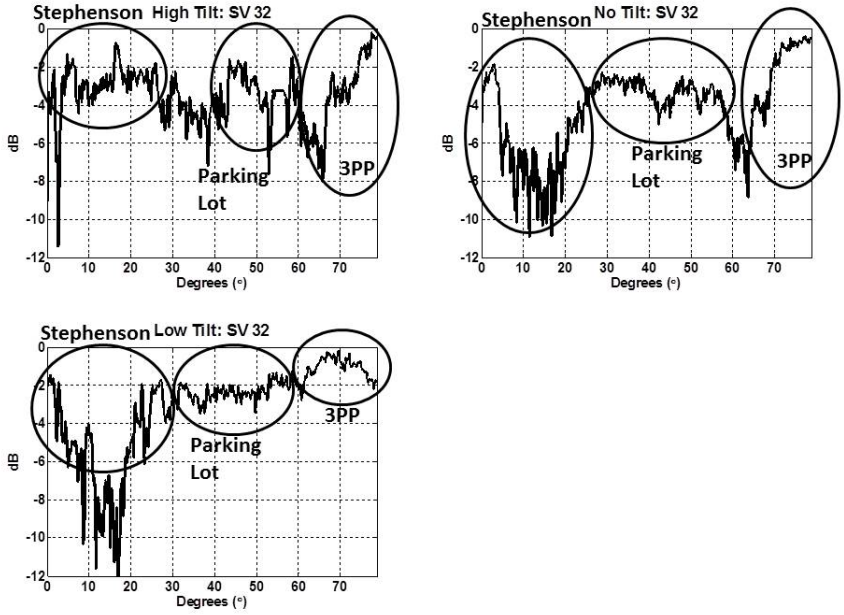

(d)

Figure 15: Test 2 results: (a) Point-of-View of Testing Area, scanned from left to right; (b) SV locations; (c) High, No, and Low Tilt of the Relative Power of SV 31 normalized in dB; (d) High, No, and Low Tilt of the Relative Power of SV 32 normalized in dB

Again, in Test 2 as in Test 1, the major targets are identified in Figure 15(a) (north of the NWC) and the SVs locations are shown in Figure 15(b). Figure 15(c) shows the relative power of SV 31, normalized in dB, as the Scanning Array was tilted toward the sky, not tilted (i.e. level with the horizon), and tilted toward the ground. Figure 15(d) is a repeat of Figure 15(c) specifically for SV 32. The Stephenson building is easily identifiable from Figure 15(c) in the first 20 seconds of data collection. Although not as easy as Figure 15(c), the building can be found in the first 20 seconds of Figure 15(d) by noting the large spikes at the 20 second mark as the array begins collecting the signals reflected from the ground. Note from Figure 15(b) that SV 32 is in front of the array which is contrary to SV 31, which is slightly behind the array and creates more reflections for the array to collect. Again, the large horizontal beamwidth mars the data received leading to small changes in between the high tilt, no tilt, and low tilt data. Many of the changes in data is possibly due to SV location data between the different scans.

5.2 Future Test Plan

Upcoming tests will include a repeat of the previous Test 1 and Test 2, this time with a horn around the GPS Array to reduce the effective horizontal beamwidth, and later, utilizing the GPS Array's beamforming and beamsteering capabilities. We expect the collected data to be different but comparable to the previously collected data, ideally with less multi-path interference in (identifiable in Tests 1 and 2) and more distinguishability between tilted scans (Test 2). Furthermore, beamsteering will lead to beam-widening at the larger off-broadside angles, but should still give desirable results.

Further tests will involve mounting the GPS Array to the underside of the wings of a UAV to perform flight data collection, which would fully realize the GPS Array's hybrid-aperture capabilities. Figure 1 provides a visual representation of the GPS Array mounted along the underside of the wings of a UAV, flying along the Y-direction to collect real-aperture data while simultaneously scanning the beam in the X-direction to collect synthetic-aperture data.

REFERENCES

[1] R. Zuo, *Bistatic Synthetic Aperture Radar Using GNSS as Transmitters of Opportunity*, PhD Thesis, University of Birmingham, UK, 2011.

[2] M. Cheriniakov (Editor), *Bistatic Radar: Emerging Technology*, Wiley, April 2008, pp. 339-361.

[3] A. Soloviev, F. V. Graas, S. Gunawardena *et al.*, "Synthetic Aperture GPS Signal Processing: Concept and Feasibility Demonstration," *Inside GNSS*, pp. 37-46b, May-June, 2009.

[4] Francis M. Czopek, Scott Shollenberger, Description and Performance of the GPS Block I and II L-Band Antenna and Link Budget, Proceedings of the 6th International Technical Meeting of the Satellite Division of The Institute of Navigation (ION GPS 1993), September 22 - 24, 1993.

[5] I. Walterscheid, T. Espeter, A. R. Brenner *et al.*, "Bistatic SAR Experiments With PAMIR and TerraSAR-X: Setup, Processing, and Image Results," *IEEE Transactions on Geoscience and Remote Sensing*, vol. 48, no. 8, pp. 3268-3279.

[6] P. Ward and J. Betz, "GPS Satellite and Characteristics," *Understanding GPS: Principles and Applications, Second Edition*¸ Artech House, Norwood, MA, 2006, pp. 113-151.

[7] K. Borre, D. Akos *et al.*, *A Software-Defined GPS and GALILEO Receiver: A Single-Frequency Approach*, Birkhäuser, Boston: 2007, pp. 69-135.